# Coprime Factorization Approach to Robust Stabilization of the Control Structures Interaction Evolutionary Model

E. S. Armstrong

**Reprinted from**

**Journal of Guidance, Control, and Dynamics**

Volume 17, Number 5, Pages 935–941

*A publication of the*
American Institute of Aeronautics and Astronautics, Inc.
370 L'Enfant Promenade, SW
Washington, DC 20024-2518

JOURNAL OF GUIDANCE, CONTROL, AND DYNAMICS
Vol. 17, No. 5, September–October 1994



# Coprime Factorization Approach to Robust Stabilization of Control Structures Interaction Evolutionary Model

Ernest S. Armstrong*
*NASA Langley Research Center, Hampton, Virginia 23681*

**Stabilization in the presence of uncertainties is a fundamental requirement in the design of feedback compensators for flexible structures. The search for the largest neighborhood around a given design plant for which a single feedback controller produces closed-loop stability can be formulated as an $H_\infty$ control problem. It has been shown that the use of normalized coprime factor plant descriptions, where the plant perturbations are defined as additive modifications to the coprime factors, leads to a closed-form expression for the maximal-neighborhood boundary allowing optimal and suboptimal $H_\infty$ compensators to be computed directly without the usual $\gamma$-iteration. This paper describes an application of normalized coprime factor stabilization theory to the computation of robustly stable compensators for the NASA Control Structures Interaction Evolutionary Model. Results indicate that the suboptimal version of the theory has the potential of providing low authority compensators that are robustly stable for significant regions of variations in design model parameters and additive unmodeled dynamics.**

## Nomenclature

| | |
|---|---|
| $(A, B, C, D)$ | = minimal state-variable realization for $G(s)$ |
| $(A_f, B_f, C_f, D_f)$ | = state-variable realization of 25-mode model in phase 0 simulation |
| $(A_t, B_t, C_t, D_t)$ | = state-variable realization for truncated system $\Delta G(s)$ in phase 0 simulation |
| $A_\delta$ | = system matrix for perturbed phase 0 simulation |
| $C_\delta$ | = output matrix in state-variable realization of perturbed phase 0 system |
| $\mathcal{F}_U(P, \Delta P)$ | = upper linear-fractional transform |
| $\mathcal{F}_L(P, K)$ | = lower linear-fractional transform |
| $G(s)$ | = $p \times m$ transfer function matrix with real-rational function elements |
| $G_A(s)$ | = $G(s)$ after augmentation by loop-shaping functions |
| $G_f(s)$ | = 50th-order design model transfer-function matrix |
| $G_\Delta(s)$ | = perturbed plant |
| $G_\delta(s)$ | = transfer function for perturbed $G(s)$ |
| $G_{\delta_A}(s)$ | = $G_\delta(s)$ after augmentation by loop-shaping functions |
| $H_\infty$ | = Hardy[a] space of complex-valued functions $F(s)$ of a complex variable $s$ that are analytic and bounded in the open right-half plane in the sense that $\sup\{\|F(s)\| : \mathrm{Re}\, s > 0\} < \infty$ |
| inf | = greatest lower bound |
| $I$ | = identity matrix of appropriate order |
| $K(s)$ | = feedback compensator for $G(s)$ |
| $K_A(s)$ | = feedback compensator for $G_A(s)$ |
| $(k, i, a)$ | = positive real parameters employed in Eq. (26) |
| $\tilde{M}, \tilde{N}$ | = factors in a left-coprime factorization of $G(s)$ |
| $\tilde{M}_A, \tilde{N}_A$ | = left-coprime factors for $G_A(s)$ |
| $\tilde{M}_{A_\delta}, \tilde{N}_{A_\delta}$ | = left-coprime factors for $G_{A_\delta}(s)$ |
| $P$ | = generalized plant transfer-function matrix |
| $\boldsymbol{RH}_\infty$ | = all asymptotically stable, proper, rational transfer-function matrices |
| $s$ | = Laplace transform variable |
| sup | = least upper bound |
| $t$ | = time variable, $t \in [0, \infty)$ |
| $u(s)$ | = Laplace transform of system input $u(t)$ |
| $W_1(s), W_2(s)$ | = transfer-function matrices used for loop shaping |
| $y(s)$ | = Laplace transform of system output $y(t)$ |
| $\gamma$ | = positive real number, $1/\varepsilon$ |
| $\gamma_{\min}$ | = positive real number, $1/\varepsilon_{\max}$ |
| $(\delta\omega)_i$ | = random numbers uniformly distributed within $[-0.01, 0.01]$, $i = 1, \ldots, 9$ |
| $(\delta\zeta)_i$ | = random numbers uniformly distributed within $[-0.1, 0.1]$, $i = 1, \ldots, 9$ |
| $\Delta P$ | = generalization perturbation |
| $\Delta G(s)$ | = perturbation to $G(s)$ |
| $\Delta\tilde{M}, \Delta\tilde{N}$ | = perturbations to left-coprime factors of $G(s)$ |
| $\Delta\tilde{M}_A, \Delta\tilde{N}_A$ | = perturbations to left-coprime factors of $G_A(s)$ |
| $\varepsilon, \varepsilon_A$ | = positive real number used as a robustness measure |
| $\varepsilon_{\max}$ | = largest value of $\varepsilon$ |
| $\zeta_i$ | = damping ratio for the $i$th mode of the phase 0 model, $i = 1, \ldots, 25$ |
| $(\zeta_p)_i$ | = perturbed value of damping ratio $\zeta_i$, $i = 1, \ldots, 9$ |
| $Z$ | = diagonal matrix of damping ratios of 25-mode phase 0 simulation model |
| $\bar{\sigma}(A)$ | = largest singular value of constant matrix $A$ |
| $\underline{\sigma}(A)$ | = smallest singular value of constant matrix $A$ |
| $\bar{\sigma}[G(s)]$ | = largest Hankel singular value of $G \in \boldsymbol{RH}_\infty$ |
| $\Phi$ | = mode-shape matrix |
| $\omega$ | = frequency, rad/s |
| $\omega_i$ | = frequency of $i$th mode in phase 0 model, rad/s |
| $(\omega_p)_i$ | = perturbed values of $\omega_i$, rad/s |
| $\Omega$ | = diagonal matrix of frequencies of 25-mode phase 0 model, rad/s |

*Superscripts*

| | |
|---|---|
| $T$ | = matrix transpose |
| $-1$ | = matrix inverse |
| $*$ | = matrix transpose with argument $s$ replaced by $-s$, e.g., $\tilde{N}^*(s) = \tilde{N}^T(-s)$ |

*Norms*

| | |
|---|---|
| $\|\cdot\|_\infty$ | = $H_\infty$ norm: $\|G(s)\|_\infty = \sup_\omega \bar{\sigma}[G(j\omega)]$ |
| $\|\cdot\|_H$ | = Hankel norm: $\|G(s)\|_H = \bar{\sigma}[G(s)]$ |

Received Feb. 1, 1993; revision received Dec. 5, 1993; accepted for publication Jan. 10, 1994. 

*Senior Research Scientist, Guidance and Control Branch.

## Introduction

IN the design of controllers for physical systems, there almost always has to be some trade-off performed between design model accuracy and mathematical complexity.[1] The more accurate analysis models often require computational time that is too excessive to qualify them as design models for control purposes. In practice, high-order nonlinear models are typically linearized about some operating condition and have their model order reduced to produce design models that conform to computational limitations or compensator implementation constraints. These practicalities introduce modeling errors in the form of unmodeled dynamics that must be accounted for in the controller design process. Additionally, parameters in the design and analysis models are not always accurately known and can cause destabilizing effects if parametric uncertainty is ignored or improperly treated.

The foregoing considerations are especially critical in the design of controllers for flexible space structures.[2,3] Space structure controller design models are generally obtained through some order reduction procedure applied to a high-order analysis model obtained from finite element techniques. The order reduction process essentially deletes a portion of the finite element model to produce a lower order controller design model. Although no longer contained in the design model, the unmodeled dynamics (represented by the deleted portion) can still be influenced by control inputs. Care must be taken in the design process so as to avoid control and observation spillover effects[3] that destabilize the unmodeled dynamics. Also, the high-order model contains parametric uncertainties in natural frequencies, damping ratios, and mode shapes and slopes that get passed through to the design model. A fundamental requirement of control law design for flexible space structures is then the attainment and preservation of closed-loop stability in the presence of unmodeled dynamics and parameter uncertainties.

Uncertainties may be viewed as perturbations about a nominal design model. If a single compensator stabilizes the nominal plant and, in addition, all systems within some neighborhood of the plant generated by the perturbations, then the compensator is said to robustly stabilize the overall family of systems.[4] The search for the largest neighborhood around a given design plant for which a single controller produces closed-loop stability can be formulated as an $H_\infty$ control problem. Glover and McFarlane[5,6] show that the use of normalized coprime factor plant descriptions, where the plant perturbations are defined as additive modifications to the coprime factors, leads to a closed-form expression for the maximal perturbation radius. The maximal radius can be computed directly in terms of the design model, thus allowing optimal and suboptimal robust compensators to be found without the usual $\gamma$-iteration of $H_\infty$ design.

This paper describes an application of the Glover-McFarlane theory to the robust control of a simulated structure configured to have many of the dynamical characteristics and controller design difficulties associated with flexible space structures. We begin with an overview of the robust stabilization problem specialized to normalized coprime factor plant descriptions. These theoretical results are then applied to the computation of robustly stable compensators for a computer simulation of the phase 0 version of the NASA Control Structures Interaction (CSI) Evolutionary Model.[7]

## Robust Stabilization Problem for Normalized Coprime Factor Plant Descriptions

Let $G(s)$ represent a $p \times m$ transfer function matrix and $\Delta G(s)$ denote some perturbation to $G(s)$, both with real rational elements. One method of modeling plant uncertainty involves the use of coprime factorizations wherein $G$ is written in coprime factor form and the system perturbations defined in terms of perturbations to the respective coprime factors. For a left-coprime factorization

$$G = \tilde{M}^{-1}\tilde{N} \tag{1}$$

the perturbed system $G_\Delta$ is given by

$$G_\Delta = (\tilde{M} + \Delta\tilde{M})^{-1}(\tilde{N} + \Delta\tilde{N}) \tag{2}$$

with

$$\Delta G = [\Delta\tilde{M}, \Delta\tilde{N}] \in \boldsymbol{RH}_\infty \tag{3}$$

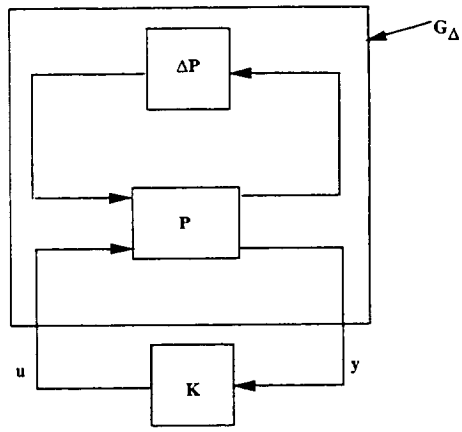


**Fig. 1 Feedback control of generalized uncertainty model.**

This uncertainty model can be represented as an upper linear-fractional transformation

$$G_\Delta = \mathcal{F}_U(P, \Delta P) = P_{22} + P_{21}\Delta P(I - P_{11}\Delta P)^{-1}P_{12} \tag{4}$$

where $\det(I - P_{11}\Delta P) \neq 0$ and

$$P = \left[\begin{array}{c|c} P_{11} & P_{12} \\ \hline P_{21} & P_{22} \end{array}\right] = \left[\begin{array}{c|c} 0 & I \\ \tilde{M}^{-1} & G \\ \hline \tilde{M}^{-1} & G \end{array}\right] \tag{5}$$

with admissible perturbations defined as

$$\Delta P = [\Delta\tilde{N}, -\Delta\tilde{M}] \in \boldsymbol{RH}_\infty \tag{6}$$

The foregoing $(P, \Delta P)$ uncertainty-model structure and the process of using feedback to stabilize and control $P$ in the presence of $\Delta P$ can be represented by the block diagram shown in Fig. 1. Employing Fig. 1, a robust stabilization problem can be posed. Viewing $G_\Delta$ as a family of perturbed models for a given class of perturbations $\Delta P$, seek a single compensator $K(s)$ that stabilizes not only $G$ (i.e., $G_\Delta$ with $\Delta P = 0$) but all members of the $G_\Delta$ family. For $P$ and $\Delta P$ given by Eqs. (5) and (6), the following robust stabilization theorem is available.[6]

*Robust stabilization theorem.* For any $P_{22}$ of $P$ given by Eq. (5) with stabilizable and detectable state-variable realization, the compensator $K(s)$ of Fig. 1 stabilizes $G_\Delta = \mathcal{F}_U(P, \Delta P)$ for all admissible $\Delta P$ such that $\|\Delta P\|_\infty < \varepsilon$ if and only if (i) $K$ stabilizes $P_{22}$ and (ii) $\|\mathcal{F}_L(P, K)\|_\infty < \varepsilon^{-1}$, where the lower linear-fractional transformation

$$\begin{aligned}\mathcal{F}_L(P, K) &= P_{11} + P_{12}K(I - P_{22}K)^{-1}P_{21} \\ &= \begin{bmatrix} K \\ I \end{bmatrix}(I - GK)^{-1}\tilde{M}^{-1}\end{aligned} \tag{7}$$

The parameter $\varepsilon$ in the theorem can be viewed as a measure of the level of robust stability for a given closed-loop system. The problem of finding the largest level of robust stability is termed the optimal robust stabilization problem and is formally stated as follows.

*Optimal robust stabilization problem.* Find the largest strictly positive number $\varepsilon = \varepsilon_{\max}$ such that, for all admissible $\Delta P$ satisfying $\|\Delta P\|_\infty < \varepsilon$, there exists a single controller that stabilizes $\mathcal{F}_U(P, \Delta P)$.

From the robust stabilization theorem,

$$\varepsilon_{\max} = \left(\inf_K \|\mathcal{F}_L(P, K)\|_\infty\right)^{-1} \tag{8}$$

where $K$ is chosen from all controllers that stabilize $P_{22}$. Computation of $\varepsilon_{\max}$ thus involves the solution of an $H_\infty$ optimization problem[8,9]; that is, find

$$\inf_K \|\mathcal{F}_L(P, K)\|_\infty = \gamma_{\min} \tag{9}$$

over all $K$ that stabilize $P_{22}$. Finding $\gamma_{\min}$ typically involves an iterative procedure to determine the smallest $\gamma$ ($= \gamma_{\min}$) such that the *suboptimal robust stabilization problem*

$$\inf_K \|\mathcal{F}_L(P, K)\|_\infty \leq \gamma \tag{10}$$

is solved. The solution of the optimal robust stabilization problem for the coprime factorization uncertainty class can also be approached in a similar manner; however, if the coprime factors of $G$ are normalized in the sense that

$$\tilde{N}(s)\tilde{N}^*(s) + \tilde{M}(s)\tilde{M}^*(s) = I \tag{11}$$

then the $\gamma$-iteration procedure can be completely avoided and the computational effort greatly reduced. It can be shown[5,6] that, for the problem of designing a controller $K$ that robustly stabilizes a plant $G$ written in normalized left-coprime factor (NLCF) form, the maximum robust stability margin is

$$\varepsilon_{\max} = (\gamma_{\min})^{-1} = \{1 - \|[\tilde{N}, \tilde{M}]\|_H^2\}^{1/2} > 0 \tag{12}$$

where the subscript $H$ refers to the Hankel norm.[10]

State-variable realizations for the suboptimal compensators with $\gamma > \gamma_{\min}$ can be found in Refs. 5 and 6. Theory and state-variable algorithms to solve the optimal problem with $\gamma = \gamma_{\min}$ can be found in Ref. 10.

## Loop Shaping Within NLCF Robust Stabilization Structure

Since $G = \tilde{M}^{-1}\tilde{N}$ is a NLCF,

$$\left\| \begin{bmatrix} K \\ I \end{bmatrix} (I - GK)^{-1}\tilde{M}^{-1} \right\|_\infty$$

$$= \left\| \begin{bmatrix} K \\ I \end{bmatrix} (I - GK)^{-1}\tilde{M}^{-1}[\tilde{M}, \tilde{N}] \right\|_\infty$$

$$= \left\| \begin{bmatrix} K(I - GK)^{-1} & K(I - GK)^{-1}G \\ (I - GK)^{-1} & (I - GK)^{-1}G \end{bmatrix} \right\|_\infty \leq \gamma \tag{13}$$

Only a certain class of weighting matrices is allowed if the exact-solution advantage enjoyed by the NLCF robust stabilization problem is to be preserved.[6]

Let $W_1(s)$ and $W_2(s)$ be system precompensator and postcompensator matrices, respectively, and define an augmented plant $G_A(s)$ by

$$G_A(s) = W_2(s)G(s)W_1(s) \tag{14}$$

Performing a NLCF robust stabilization design with $G$ replaced by $G_A$ yields a dynamic compensator $K_A(s)$ robustly stabilizing $G_A$. Figure 2a gives a block diagram illustrating this loop-shaping procedure. Simple block manipulation yields Fig. 2b, which shows that the corresponding compensator $K$ to be applied to the unshaped plant $G$ is

$$K(s) = W_1(s)K_A(s)W_2(s) \tag{15}$$

We then have

$$(\varepsilon_{A_{\max}})^{-1} = \left(1 - \|[\tilde{N}_A, \tilde{M}_A]\|_H^2\right)^{-1/2}$$

$$= \inf_{K_A} \left\| \begin{bmatrix} K_A \\ I \end{bmatrix} (I - G_AK_A)^{-1}[I, G_A] \right\|_\infty$$

$$= \inf_K \left\| \begin{bmatrix} W_1^{-1}K(I - GK)^{-1}W_2^{-1} & W_1^{-1}K(I - GK)^{-1}GW_1 \\ W_2(I - GK)^{-1}W_2^{-1} & W_2(I - GK)^{-1}GW_1 \end{bmatrix} \right\|_\infty \tag{16}$$

which indicates a weighting configuration that can be applied to the elements of Eq. (13) if the exact-solution structure is to be preserved. In general, if other weighting configurations are desired, the normal $H_\infty$ $\gamma$-iteration procedure is required.

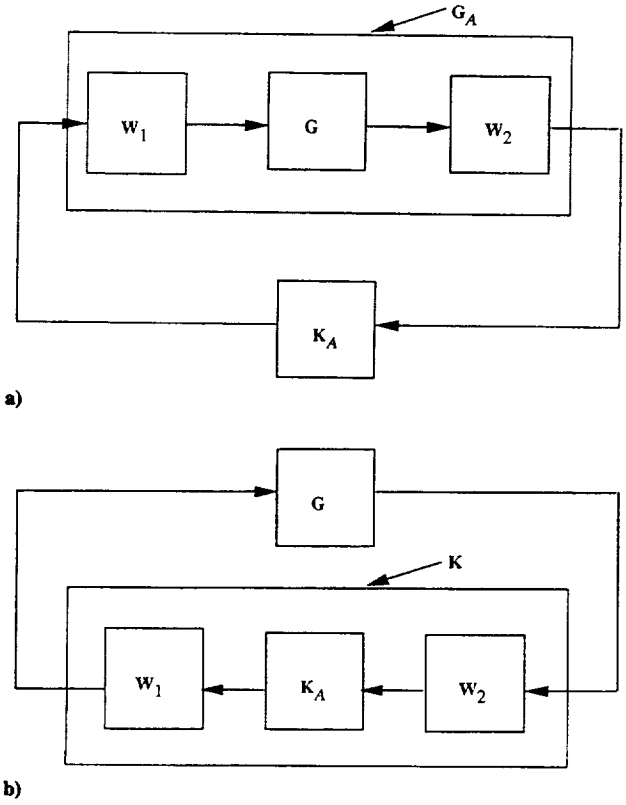


**Fig. 2 Loop-shaping procedure: a) compensator for shaped plant, $G_A(s)$ and b) equivalent compensator for unshaped plant, $G(s)$.**

## Robust Stabilization of Phase 0 Evolutionary Model

In this section, the robust stabilization theory for a plant modeled in NLCF form is applied to produce compensators for the control of a computer model of a laboratory structure having many of the characteristics and design difficulties associated with flexible space structures.

### Description of Phase 0 Model

The CSI Evolutionary Model is a laboratory testbed concept in which a sequence of testbeds is evolved with each new facility having more challenging dynamics and control characteristics than the previous. The testbeds are to be designed and constructed at the NASA Langley Research Center for the experimental validation of control techniques and integrated design methodology developed under Langley's CSI program.[11] The phase 0 model was the first testbed to be constructed under this program. Unfortunately, the phase 0 model is no longer in existence at Langley. However, many useful studies were performed using the phase 0 model,[12-14] and its data base has been archived and is still available for this and future studies. A schematic of the phase 0 structure is shown in Fig. 3 and a detailed description may be found in Ref. 7.

The phase 0 structure consisted of two vertical towers and two horizontal booms attached to a central 62-bay truss main section with each bay a 10-in. cube. The structure was suspended from the laboratory ceiling by springs and two long cables designed to minimize the interaction between the suspension and the structural modes. A laser source was mounted at the top of the taller vertical tower and a 16-ft reflector with a mirrored surface mounted on the other tower. The laser beam could be reflected by the mirrored surface onto a detector surface above the reflector. The total structural weight was 741 lb. Eight proportional bidirectional gas thrusters (air jets) provided the input force actuation, whereas eight nearly collocated servo accelerometers provided output measurements.

Global line-of-sight pointing studies have been performed using the laser targeting system.[14] This study will only be directly concerned with vibration suppression about a given operating point and will not treat laser targeting as such. However, vibration suppression

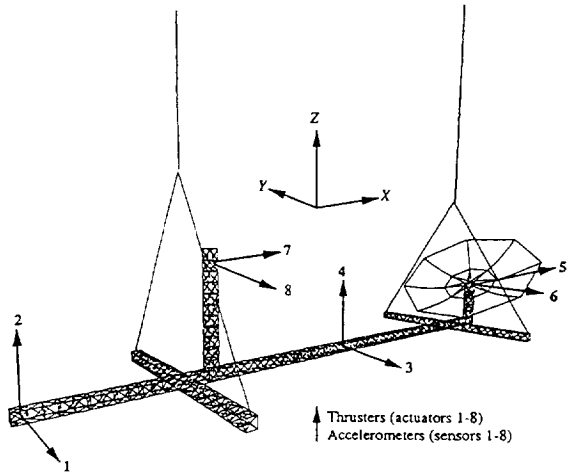


**Fig. 3 Schematic of phase 0 evolutionary model.**

of the laser tower modes will be a critical part of our design requirements since damping of the laser tower structure was a troublesome issue in previous laboratory tests.

The phase 0 model had six nonstructural modes (due to suspension) and many significant elastic modes. The NASTRAN finite element model consisted of 3560 degrees of freedom.[7] A total of 86 modes with frequencies below 50 Hz were selected as a truth or evaluation model. A reduced-order model consisting of 25 modes, selected from the 86 modes through a controllability and observability analysis, was used for the controller design model. Table 1 shows the frequency range of these 25 modes in hertz. Frequencies of the first six pendulum/suspension modes, brought about by the cable suspension in a 1 $g$ environment, range from 0.147 to 0.874 Hz. It was observed in the laboratory that the true damping ratios probably lie between 0.1 and 1.0%. For simulation and controller design purposes, previous theoretical studies with experimental validation[12] have demonstrated that a 0.5% nominal value adequately describes modes below 2 Hz to within an accuracy of 10%. Frequencies below 2 Hz in the finite element model can be taken to be accurate to within 1%.[14]

Using data from the finite element analysis, a dynamical mathematical model in the modal coordinate system can be constructed. A 50th-order state-variable realization of this model (with transfer matrix denoted by $G_f$ ) will appear as $(A_f, B_f, C_f, D_f)$, where

$$A_f = \begin{bmatrix} 0 & I \\ -\Omega^2 & -Z \end{bmatrix} \qquad B_f = \begin{bmatrix} 0 \\ \Phi^T \end{bmatrix}$$

$$C_f = [0,\ \Phi]A_f \qquad D_f = \Phi\Phi^T \tag{17}$$

with

$$\Omega = \text{diag}(\omega_1, \omega_2, \ldots, \omega_{25}) \tag{18}$$

$$Z = \text{diag}(2\zeta_1\omega_1, 2\zeta_2\omega_2, \ldots, 2\zeta_{25}\omega_{25}) \tag{19}$$

and $\Phi$ is an $8 \times 25$ matrix of mode shapes. In Eqs. (18) and (19), $\omega_i$ denotes frequency and $\zeta_i = 0.005$ damping ratio for $i = 1, \ldots, 25$. Eigenvalues of $A_f$ are given in Table 1. Since the damping ratios are small, the frequencies in radians per second are closely approximated by the imaginary parts of the eigenvalues.

In flexible structures, higher frequency modes are more difficult to accurately measure and compute. For the phase 0 structure, the finite element model provided reasonably accurate natural frequency and damping values for modes below 2 Hz. However, higher frequency modes, beginning with the 10th mode at 2.3 Hz, are not accurately known.[14] In this design, only modes with frequencies up to 14 rad/s are used to form the compensator design model and

**Table 1 Phase 0 model open-loop system characteristics**

| Mode no. | Eigenvalue (Re, ±Im) | Frequency, Hz |
|---|---|---|
| 1 | $(-4.622 \times 10^{-3}, 9.243 \times 10^{-1})$ | 0.147 |
| 2 | $(-4.682 \times 10^{-3}, 9.365 \times 10^{-1})$ | 0.149 |
| 3 | $(-4.876 \times 10^{-3}, 9.752 \times 10^{-1})$ | 0.155 |
| 4 | $(-2.294 \times 10^{-2}, 4.587)$ | 0.730 |
| 5 | $(-2.349 \times 10^{-2}, 4.698)$ | 0.748 |
| 6 | $(-2.746 \times 10^{-2}, 5.491)$ | 0.874 |
| 7 | $(-4.629 \times 10^{-2}, 9.258)$ | 1.474 |
| 8 | $(-5.460 \times 10^{-2}, 1.092 \times 10)$ | 1.738 |
| 9 | $(-5.916 \times 10^{-2}, 1.183 \times 10)$ | 1.883 |
| 10 | $(-7.230 \times 10^{-2}, 1.446 \times 10)$ | 2.301 |
| 11 | $(-8.918 \times 10^{-1}, 1.783 \times 10)$ | 2.838 |
| 12 | $(-1.261 \times 10^{-1}, 2.522 \times 10)$ | 4.015 |
| 13 | $(-1.267 \times 10^{-1}, 2.534 \times 10)$ | 4.032 |
| 14 | $(-1.321 \times 10^{-1}, 2.642 \times 10)$ | 4.206 |
| 15 | $(-1.380 \times 10^{-1}, 2.760 \times 10)$ | 4.392 |
| 16 | $(-1.728 \times 10^{-1}, 3.457 \times 10)$ | 5.501 |
| 17 | $(-1.941 \times 10^{-1}, 3.883 \times 10)$ | 6.180 |
| 18 | $(-1.958 \times 10^{-1}, 3.915 \times 10)$ | 6.231 |
| 19 | $(-2.033 \times 10^{-1}, 4.066 \times 10)$ | 6.471 |
| 20 | $(-2.095 \times 10^{-1}, 4.191 \times 10)$ | 6.670 |
| 21 | $(-2.316 \times 10^{-1}, 4.632 \times 10)$ | 7.372 |
| 22 | $(-2.605 \times 10^{-1}, 5.211 \times 10)$ | 8.293 |
| 23 | $(-2.817 \times 10^{-1}, 5.634 \times 10)$ | 8.966 |
| 24 | $(-3.922 \times 10^{-1}, 7.845 \times 10)$ | 12.49 |
| 25 | $(-5.294 \times 10^{-1}, 1.059 \times 10^{2})$ | 16.85 |

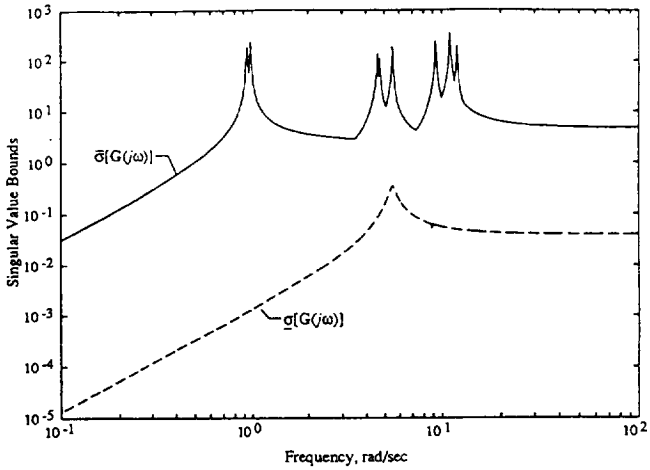


**Fig. 4 Unweighted open-loop nominal system $G(s)$.**

modes with higher frequencies are used to simulate unmodeled dynamics. Modes above mode 9 are truncated from the 25-mode model and accounted for as an additive uncertainty in the design process. The matrix $G_f$ now appears as

$$G_\Delta = G_f = G + \Delta G \tag{20}$$

$$G = C(sI_{18} - A)^{-1}B + D \tag{21}$$

and

$$\Delta G = C_t(sI_{32} - A_t)^{-1}B_t + D_t \tag{22}$$

Numerical data for $(A, B, C, D)$ and $(A_t, B_t, C_t, D_t)$ are given in Appendix C of Ref. 15. Figures 4 and 5 show individual frequency response (sigma) plots for $G$ and $\Delta G$.

### Design Approach

A controller achieving robust vibration suppression is the goal of this study. The control design should increase the damping of all the pseudo rigid-body (suspension) and structural modes of the design model $G$. The closed-loop system must also possess stability robustness with respect to unmodeled structural modes, of which $\Delta G$

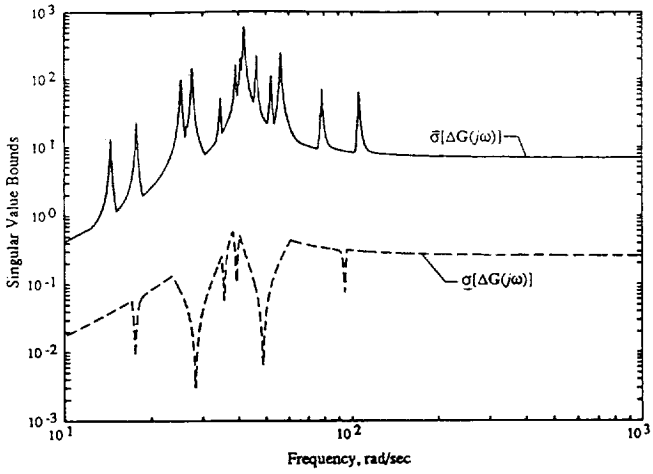


**Fig. 5 Truncated system $\Delta G(s)$.**

from Eq. (22) is taken as a representative sample, and to the parametric uncertainties generated by the expected errors in frequency (1%) and damping ratios (10%) in the design model.

In the application of the NLCF robust stabilization theory to follow, stability robustness to additive unmodeled dynamics is incorporated by use of the weighting matrices in Eq. (14) and analyzed through examination of closed-loop conditions for stability robustness,[8]

$$\|\Delta GK(I - GK)^{-1}\|_\infty < 1 \tag{23}$$

or the more conservative sufficient condition for Eq. (23),

$$\bar{\sigma}[\Delta G(s)]\bar{\sigma}[K(I - GK)^{-1}(s)] < 1 \tag{24}$$

for $s = j\omega$, $\omega \in [0, \infty)$. The design parameters in the weighting matrices are adjusted so that condition (23) is satisfied with a margin of at least 40% and no destabilization of the closed-loop system is experienced from the expected parametric variations in the open-loop design system. Thereafter, within the remaining freedom allowed, the parameters are adjusted to achieve the largest increase in damping in the suspension and structural modes of $G(s)$.

**Loop-Shaping Procedures**

Optimal compensator and central suboptimal compensators were computed. Both compensators, when applied to $G$ in the feedback fashion of Fig. 2, enhanced the stability of $G$ but grossly violated spillover condition (23) with $\Delta G$ given by Eq. (22). Failure to satisfy condition (23) was primarily caused by the lack of free parameters for adjustment in the algorithms and the fact that $G(s)$ is not strictly proper, in which case both optimal and suboptimal compensators will not be strictly proper.

It was found that the spillover problem could be resolved through incorporation of loop-shaping functions of the form (14). Weighting functions employed were

$$W_1(s) = I_8 \tag{25}$$

and

$$W_2(s) = k/(s + a)^i I_8 \tag{26}$$

The positive real parameters $a$, $i$, and $k$ are adjusted from observation of condition (24) with the compensator (15). The parameter $a$ is chosen such that a plot of the inverse of $\bar{\sigma}[K(I - GK)^{-1}(j\omega)]$ vs. $\omega \in [0, \infty)$ breaks upward before $\omega = 14$ rad/s, the approximate frequency at which the $\Delta G$ dynamics become predominant. The parameter $i$ roughly controls the slope of the upward break and was taken as $i = 1$ or $i = 2$. The quantity $k$ adjusts the magnitude of $W_2(s)$ and, in the studies to follow, ranged between 0.08 and 4.0. Increasing the parameter $k$ moves the closed-loop eigenvalues of the controllable modes of the design model further into the complex left-hand plane but also increases the potential of destabilizing spillover into the modes of $A_t$.

**Analysis of Robustness to Structured Perturbations**

Values of natural frequency are assumed to be accurate to within 1% and values of damping ratio to within 10% for modes 1–9 below 2 Hz.[12,14] In order to evaluate the compensators for perturbations in frequencies and damping ratios within these ranges, the frequencies $\omega_i$ and damping ratios $\zeta_i$ in the $A$-matrix of the nine-mode design model were replaced by perturbed values $(\omega_p)_i$ and $(\zeta_p)_i$ given by

$$(\omega_p)_i = \omega_i + (\delta\omega)_i\omega_i \tag{27}$$

and

$$(\zeta_p)_i = \zeta_i + (\delta\zeta)_i\zeta_i \tag{28}$$

for $i = 1, \ldots, 9$. In Eqs. (27) and (28), $(\delta\omega)_i$ and $(\delta\zeta)_i$, $i = 1, \ldots, 9$, are random variables uniformly distributed within $[-0.01, +0.01]$ and $[-0.1, +0.1]$, respectively. The new perturbed system matrix is denoted by $A_\delta$. If $G(s)$ is given by Eq. (21), the transfer matrix for the perturbed system is

$$G_\delta(s) = C_\delta(sI_{18} - A_\delta)^{-1}B + D \tag{29}$$

where

$$C_\delta = CA^{-1}A_\delta \tag{30}$$

to reflect acceleration measurements.

With

$$G_A(s) = W_2(s)G(s)W_1(s) \tag{31}$$

$$G_{\delta_A}(s) = W_2(s)G_\delta(s)W_1(s) \tag{32}$$

find normalized left-coprime factors such that

$$G_A(s) = (\tilde{M}_A)^{-1}\tilde{N}_A \tag{33}$$

$$G_{\delta_A}(s) = (\tilde{M}_{\delta_A})^{-1}\tilde{N}_{\delta_A} \tag{34}$$

Define

$$\Delta P = [\Delta\tilde{N}_A, -\Delta\tilde{M}_A] \tag{35}$$

where

$$\Delta\tilde{M}_A = \tilde{M}_{\delta_A} - \tilde{M}_A \tag{36}$$

$$\Delta\tilde{N}_A = \tilde{N}_{\delta_A} - \tilde{N}_A \tag{37}$$

If $\|\Delta P\|_\infty < \varepsilon_A$, then the compensators, in addition to stabilizing $G(s)$, also stabilize the perturbed system. No computations are made to measure the effect of the parametric perturbations on the unperturbed closed-loop damping ratios.

**Compensator Design**

*Optimal Compensator*

It was found[15] that, since the optimal compensator was not strictly proper, $i = 2$ provided faster roll-off and best allowed the satisfaction of conditions (23) and (24). A representative optimal compensator used $(k, i, a) = (0.1, 2, 0.5)$. After scaling each channel of $G$ by $0.1/(s + 0.5)^2$, it was found that $\varepsilon_{A_{max}} = 0.6749$.

Over 2000 realizations of Eqs. (27) and (28) were computed for the optimal compensator and the corresponding $\Delta P$ transfer matrices [given by Eq. (35)] tested for satisfaction of $\|\Delta P\|_\infty < \varepsilon_{A_{max}}$. No violations were encountered. Values of $\|\Delta P\|_\infty$ ranged between 0.1728 and 0.5888 with a mean of 0.4627 and standard deviation of 0.0726. A frequency analysis of condition (23) indicates that mode 20 (the laser tower mode) at 41.9 rad/s (6.7 Hz) is the mode most likely to experience destabilizing spillover. This property has also been observed experimentally in previous studies.[12] The analysis also indicated an additive stability robustness margin of about 97%. This ultraconservative margin for additive stability robustness was forced by the desire to also have a compensator that guaranteed stability robustness to expected parametric uncertainties in frequencies and damping ratios. For the same values of $i$ and $a$, if $k$ is increased

**Table 2 Eigenvalues of $K_A(s)$ compensator system matrix**

| Real | Complex (Re, ±Im) |
|---|---|
| −0.1 (multiplicity 8) | (−2.296, 4.230) |
| −0.1612 | $(-2.366 \times 10^{-1}, 4.690)$ |
| −0.2945 | (−1.859, 5.232) |
| −0.4769 | (−2.339, 8.859) |
| −1.8518 | (−3.535, 9.659) |
| −3.1977 | $(-1.408, 1.103 \times 10)$ |
| −6.8123 | |

Note: Reflects suboptimal studies; $(k, i, a) = (0.5, 1, 0.1)$, $\varepsilon_{A_{max}} = 0.6670$, $\varepsilon_A = 0.9\varepsilon_{A_{max}}$.

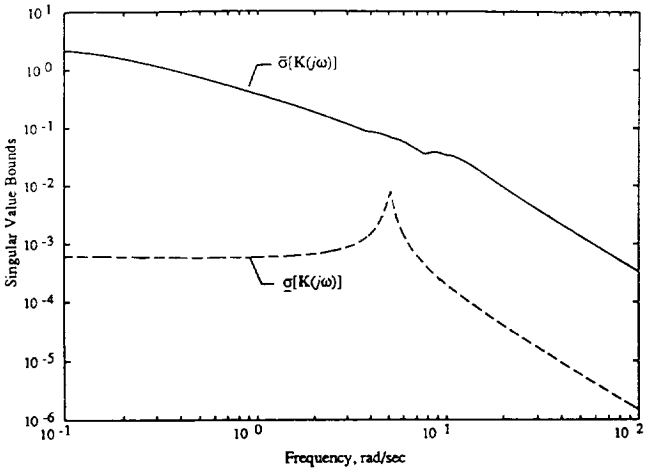


**Fig. 6 Suboptimal compensator $K(s)$.**

to 2.0, then a more reasonable margin of 43% is obtained. However, $k = 2.0$ produced $\varepsilon_{A_{max}} = 0.4856$, and this reduced value of $\varepsilon_{A_{max}}$ leads to violations occurring greater than 40% of the time in the random tests for $\|\Delta P\|_\infty < \varepsilon_{A_{max}}$. For fixed values of $i$ and $a$, decreasing $k$ increases $\varepsilon_{A_{max}}$ and decreases $\|\Delta P\|_\infty$. A value of $k$ allowing a sufficiently wide "gap" between the two quantities is required when specific ranges of parametric variations are considered.

The (0.1, 2, 0.5) compensator, when applied in the closed-loop manner of Fig. 2 to the 50th-order system $G_\Delta$, leaves the open-loop eigenvalues essentially unchanged except for modes 1–3. Optimal compensators with better stability augmentation can be obtained at the expense of violations in robust stability due to parametric variations in frequencies and damping ratios of the design model.

*Suboptimal Compensators*

Central suboptimal compensators computed from strictly proper systems $G_A(s)$ are strictly proper, whereby lower order weighting functions (than those used in the foregoing optimal compensator studies) can be employed without difficulty in satisfying the additive robustness conditions. Suboptimal compensator studies[15] were performed using $i = 1$ and $\varepsilon_A = 0.9\varepsilon_{A_{max}}$ from which a representative result had $(k, i, a) = (0.5, 1, 0.1)$. After scaling each channel of $G$ by $0.5/(s+0.1)$, it was found that $\varepsilon_{A_{max}} = 0.667$. Table 2 gives the eigenvalues of the Hurwitz system matrix from a state-variable realization of $K_A(s)$. The order of the final compensator $K$ is 34. Figure 6 shows singular-value bounds for the compensator $K(s)$.

Again, over 2000 realizations of Eqs. (27) and (28) were computed for the suboptimal compensator and the corresponding $\Delta P$ transfer matrices tested for satisfaction of $\|\Delta P\|_\infty < \varepsilon_{A_{max}}$ with no violations encountered. Values of $\|\Delta P\|_\infty$ ranged between 0.0561 and 0.5595 with a mean of 0.2798 and standard deviation of 0.0907. The expected variations in frequency and damping ratio of 1 and 10%, respectively, are apparently close to the upper bounds for robust stability for $k = 0.5$. Increasing the variations to 1.5% in frequency and 15% in damping ratio causes violations about 6% of the time.

**Table 3 Closed-loop eigenvalues of design model controlled by compensator $K(s)$**

| Open-loop mode no. | Eigenvalues (Re, ±Im) | Damping ratio, $\zeta$ |
|---|---|---|
| 1[a] | | |
| 2[a] | | |
| 3 | $(-2.610 \times 10^{-1}, 8.872 \times 10^{-1})$ | 0.2822 |
| 4 | $(-5.216 \times 10^{-1}, 4.620)$ | 0.1122 |
| 5 | $(-1.767 \times 10^{-1}, 4.671)$ | 0.0378 |
| | or | or |
| | $(-9.510 \times 10^{-2}, 4.653)$ | 0.0204 |
| 6 | $(-4.760 \times 10^{-1}, 5.480)$ | 0.0865 |
| 7 | $(-6.248 \times 10^{-1}, 9.237)$ | 0.0675 |
| 8 | $(-9.416 \times 10^{-1}, 1.086 \times 10)$ | 0.0838 |
| 9 | $(-4.921 \times 10^{-1}, 1.178 \times 10)$ | 0.0417 |
| 10 | $(-8.062 \times 10^{-2}, 1.447 \times 10)$ | 0.0056 |
| 11 | $(-1.056 \times 10^{-1}, 1.785 \times 10)$ | 0.0059 |
| 12 | $(-1.266 \times 10^{-1}, 2.522 \times 10)$ | 0.0050 |
| 13 | $(-1.391 \times 10^{-1}, 2.538 \times 10)$ | 0.0055 |
| 14 | $(-1.336 \times 10^{-1}, 2.643 \times 10)$ | 0.0051 |
| 15 | $(-1.606 \times 10^{-1}, 2.766 \times 10)$ | 0.0058 |
| 16 | $(-1.747 \times 10^{-1}, 3.458 \times 10)$ | 0.0050 |
| 17 | $(-1.953 \times 10^{-1}, 3.884 \times 10)$ | 0.0050 |
| 18 | $(-2.038 \times 10^{-1}, 3.919 \times 10)$ | 0.0052 |
| 19 | $(-2.133 \times 10^{-1}, 4.071 \times 10)$ | 0.0052 |
| 20 | $(-2.122 \times 10^{-1}, 4.194 \times 10)$ | 0.0051 |
| 21 | $(-2.334 \times 10^{-1}, 4.634 \times 10)$ | 0.0050 |
| 22 | $(-2.623 \times 10^{-1}, 5.212 \times 10)$ | 0.0050 |
| 23 | $(-2.895 \times 10^{-1}, 5.639 \times 10)$ | 0.0051 |
| 24 | $(-3.924 \times 10^{-1}, 7.845 \times 10)$ | 0.0050 |
| 25 | $(-5.295 \times 10^{-1}, 1.059 \times 10^2)$ | 0.0050 |

Note: Reflects suboptimal studies; $(k, i, a) = (0.5, 1, 0.1)$, $\varepsilon_{A_{max}} = 0.6670$, $\varepsilon_A = 0.9\varepsilon_{A_{max}}$.
[a]Not discernible from data.

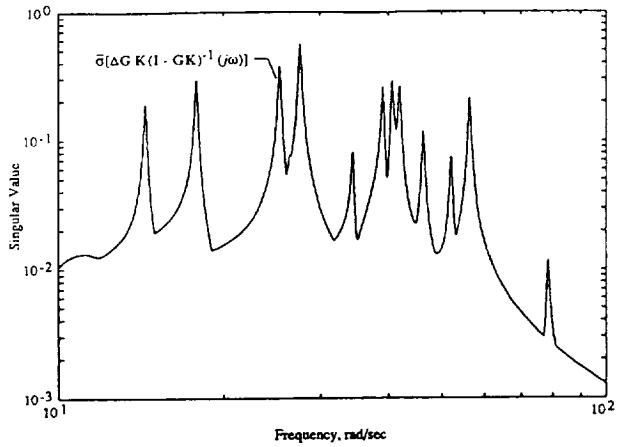


**Fig. 7 Robustness condition (23) for suboptimal compensator $K(s)$.**

Satisfaction of condition (23) is shown in Fig. 7. The peak value of the singular-value curve Fig. 7 is 0.562, indicating an additive stability robustness margin of about 44%.

The suboptimal compensator was also applied to the control of the 50th-order system $G_\Delta$ and an eigenvalue analysis performed. Results are given in Table 3. The real parts of the eigenvalues for modes 10–25 are not significantly changed from the corresponding values of Table 1, indicating that the additive robustness conditions are satisfied. The eigenvalue data gave two eigenvalues with imaginary parts close to the imaginary part of open-loop mode 5. Both are shown in Table 3. It is possible that the entry with the largest real part is the closed-loop eigenvalue of mode 5 since this mode is the least controllable and observable of the first nine modes. No correlation could be made for modes 1 and 2.

*Evaluation Model Simulations*

The suboptimal compensator was applied to the control of the full 86-mode evaluation phase 0 model subjected to a transient

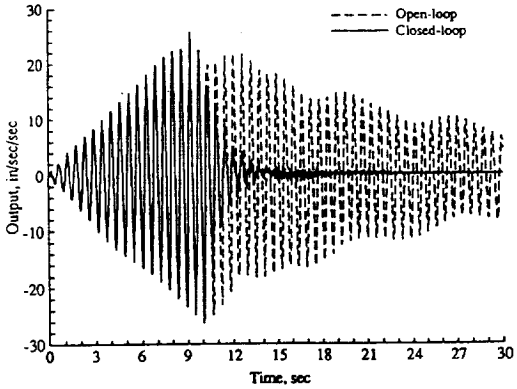


**Fig. 8 Accelerometer 7 output time history for suboptimal compensator $K(s)$.**

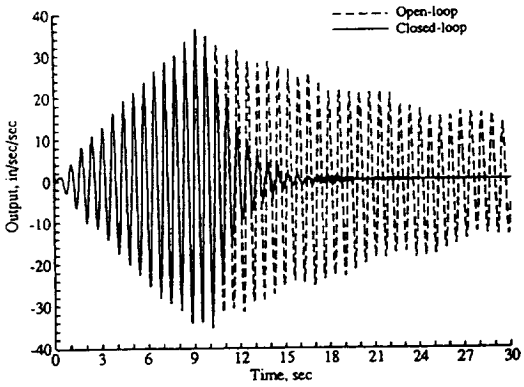


**Fig. 9 Accelerometer 8 output time history for suboptimal compensator $K(s)$.**

input disturbance. The simulation consisted of applying an excitation input sequence for the first 9 s, allowing 1 s of free decay and then applying a controller at the 10-s mark for a total duration of 30 s. The input sequence consisted of harmonic forces designed to excite two pendulum modes (modes 1 and 3) and the first two bending modes (modes 7 and 8) using a single actuator for each mode. Specifically, actuators 1 (mode 7), 2 (mode 8), 6 (mode 3), and 7 (mode 1) were excited with signals of 1.474, 1.738, 0.155, and 0.147 Hz, respectively. No actuator dynamics were considered.

The compensators were discretized at a sampling rate of 133 Hz. This is the same input sequence and sampling rate employed in experimental investigations[12] using the actual phase 0 structure. Figures 8 and 9 show output time histories for accelerometers 7 and 8 at the laser tower location. The suboptimal responses compare favorably with other compensators[12,14] designed with performance issues in mind.

## Concluding Remarks

A robust stabilization approach based on the use of normalized coprime factor plant descriptions has been applied to produce vibration-suppression controllers for a simulated model of the CSI phase 0 evolutionary model. The study indicates that, when requiring the compensators to satisfy the design objectives of stability augmentation, robust stability to unmodeled dynamics appearing as additive perturbations, and robustness to structured parametric variations, the optimal robust compensators can be overly conservative with marginal stability augmentation, whereas the suboptimal compensators are not. For the class of flexible-structure applications considered, the suboptimal version of the McFarlane-Glover theory provides a viable approach for the computation of low authority controllers providing robust stability augmentation. These controllers may need to be supplemented with high authority loops to meet additional performance objectives.

## References

[1]Maciejowski, J. M., *Multivariable Feedback Design*, Addison-Wesley, New York, 1989.

[2]Joshi, S. M., *Control of Large Flexible Space Structures*, Vol. 131, Lecture Notes in Control and Information Sciences, Springer-Verlag, New York, 1989.

[3]Balas, M. J., "Trends in Large Space Structures Control Theory: Fondest Hopes, Wildest Dreams," *IEEE Transactions on Automatic Control*, Vol. AC-27, No. 3, 1982, pp. 522–535.

[4]Dorato, P., and Yedavalli, R. C. (eds.), *Recent Advances in Robust Control*, IEEE, New York, 1990.

[5]Glover, K., and McFarlane, D. C., "Robust Stabilization of Normalized Coprime Factor Plant Descriptions with $H_\infty$-Bounded Uncertainty," *IEEE Transactions on Automatic Control*, Vol. AC-34, No. 8, 1989, pp. 821–830.

[6]McFarlane, D. C., and Glover, K., *Robust Controller Design Using Normalized Coprime Factor Plant Descriptions*, Vol. 138, Lecture Notes in Control and Information Sciences, Springer-Verlag, New York, 1990.

[7]Belvin, W. K., Elliott, K. B., Horta, L. G., Bailey, J. P., Bruner, A. M., Sulla, J. L., Won, J., and Ugoletti, R. M., "Langley's Evolutionary Model: Phase 0," NASA TM 104165, Langley Research Center, Nov. 1991.

[8]Francis, B. A., *A Course in $H_\infty$ Control Theory*, Vol. 88, Lecture Notes in Control and Information Sciences, Springer-Verlag, New York, 1987.

[9]Doyle, J. C., Glover, K., Khargonekar, P. D., and Francis, B. A., "State-Space Solutions to Standard $\mathcal{H}_2$ and $\mathcal{H}_\infty$ Control Problems," *IEEE Transactions on Automatic Control*, Vol. AC-34, No. 8, 1989, pp. 831–847.

[10]Glover, K., "All Optimal Hankel-Norm Approximations of Linear Multivariable Systems and Their $L^\infty$-Error Bounds," *International Journal of Control*, Vol. 39, No. 6, 1984, pp. 1115–1193.

[11]Newsom, J. R., Layman, W. E., Waites, H. B., and Hayduk, R. J., "The NASA Controls-Structures Interaction Program," NASA TM 102752, 1990.

[12]Lim, K. B., Maghami, P. G., and Joshi, S. M., "Comparison of Controller Designs for an Experimental Flexible Structure," *IEEE Control Systems Magazine*, Vol. 12, No. 3, 1992, pp. 108–118.

[13]Maghami, P. G., Joshi, S. M., and Armstrong, E. S., "An Optimization-Based Integrated Controls-Structures Design Methodology for Flexible Space Structures," NASA TP 3283, Nov. 1992.

[14]Lim, K. B., and Balas, G. J., "Line-of-Sight Control of the CSI Evolutionary Model: $\mu$ Control," *Proceedings of the American Control Conference*, 1992, pp. 1996–2000.

[15]Armstrong, E. S., "Robust Controller Design for Flexible Structures Using Normalized Coprime Factor Plant Descriptions," NASA TP 3325, May 1993.